Biosensors and Bioelectronics 135 (2019) 8–13

Contents lists available at ScienceDirect

Biosensors and Bioelectronics

journal homepage: www.elsevier.com/locate/bios

An ultrasensitive electrochemiluminescence biosensor for MicroRNA detection based on luminol-functionalized Au NPs@ZnO nanomaterials as signal probe and dissolved O_2 as coreactant

Xiaoli Zhang, Weimin Li, Ying Zhou, Yaqin Chai**, Ruo Yuan*

Key Laboratory of Ministry of Education of Luminescence and Real-Time Analytical Chemistry, School of Chemistry and Chemical Engineering, Southwest University, Chongqing, 400715, PR China

ARTICLE INFO

Keywords:
ZnO as coreaction accelerator
Dissolved O_2 as coreactant
miRNA-21 detection
DNA dendrimer

ABSTRACT

In this work, the ZnO nanostars with excellent catalytic performance were firstly used as the coreaction accelerator of luminol-O_2 system to construct a biosensor for ultrasensitively detecting microRNA-21 (miRNA-21) in cancer cells. Specifically, ZnO nanostars could expedite the reduction of dissolved O_2, generating more reactive oxygen species (ROSs) to extremely promote electrochemiluminescence (ECL) luminous efficiency of luminol. Thus luminol-functionalized Au NPs@ZnO (L-Au NPs@ZnO) nanomaterials were employed as signal probe to fabricate sensing nano-platform for achieving significant ECL emission as "signal on" state. Moreover, upon the addition of a tiny minority of target miRNA-21, massive ferrocene (Fc) could be immobilized on the sensing interface through hybridization chain reaction (HCR) triggered-DNA dendrimers self-assembly, in which Fc consumed dissolved O_2 for prominently quenching the ECL emission of signal probe and then reached a "signal off" state. As a result, the biosensor performed a good linearity in 100 aM – 100 pM and a low limit of detection (LOD) down to 18.6 aM. In general, this work utilized a new coreaction accelerator as an efficient amplification approach for ultrasensitively detecting target analyses, providing a promising approach in luminol-centric ECL bioanalysis fields.

1. Introduction

Luminol, as a classical significant electrochemiluminescence (ECL) luminophore, has inherent advantages of no toxic, low oxidation potential and high light-emitting quantum yield (Richter, 2004; Gu et al., 2015; Hao et al., 2017). However, it is difficult to immobilize luminol into the sensing interface due to its lack of active group (Cui et al., 2007), meantime, it extremely depended on H_2O_2 as coreactant to enhance the ECL luminous intensity, whereas H_2O_2 has defects of instability in test solution and detrimental to biology (Liu et al., 2016). Therefore, in order to improve the ECL signal of luminol-centric biosensor, it is of great significance to achieve the immobilization of luminol to H_2O_2-free strategies. In recent years, because dissolved O_2 has identical characteristic with H_2O_2 in generating reactive oxygen species (ROSs) to catalyze luminophore (Qiao et al., 2018), it could be a desirable candidate as a nontoxic coreactant to apply in the fabrication of ECL biosensors. However, the transformation efficiency of dissolved O_2 to ROSs on the interface of glassy carbon electrode (GCE) was limited, resulting in a weak ECL emission of luminol-O_2 system. Therefore, it is critical to boost the reduction efficiency of dissolved O_2 for generating more ROSs on the GCE surface to prominently enhance ECL emission of luminol-O_2 system.

In recent years, coreaction accelerator was introduced for catalyzing coreactant to generate more tremendous reactive radicals, which remarkably improved the luminous efficiency of luminophore (Lei et al., 2018; Sun et al., 2018). Very recently, we utilized Au-Ag-Pt heteronanostructures (AAPHNs) as coreaction accelerator to improve the ECL intensity of luminol-O_2 system for peptide sensitive detection (Wu et al., 2018). Nevertheless, luminol was away from AAPHNs as coreaction accelerator which caused longer electronic transmission distance between the generated ROSs on AAPHNs surface and luminol, resulting in more energy loss and limiting the coreaction acceleration efficiency of AAPHNs to luminol-O_2 system. Herein, shortening the distance between coreaction accelerator and luminophore would reduce electronic transmission distance and decrease energy loss for improving coreaction acceleration efficiency. ZnO, one kind band gap

* Corresponding author.
** Corresponding author.
E-mail addresses: yqchai@swu.edu.cn (Y. Chai), yuanruo@swu.edu.cn (R. Yuan).

https://doi.org/10.1016/j.bios.2019.04.004
Received 20 February 2019; Received in revised form 27 March 2019; Accepted 1 April 2019
Available online 06 April 2019
0956-5663/

metal oxide semiconductor, could promote the generation of ROSs through aggregating and catalyzing the decomposition of dissolved O_2 around the ZnO in test solution (Sirelkhatim et al., 2015; He et al., 2014). Compared with traditional ZnO nanoparticals, ZnO nanostars with larger surface area could effectively catalyze the generation of ROSs through dissolved O_2. In this work, ZnO nanostars were firstly employed as coreaction accelerator with dissolved O_2 as endogenous coreactant to significantly enhance the ECL intensity of luminol. Meantime, luminol was directly modified on the surface of ZnO nanostars, which could not only extremely shorten the electron-transfer path for less energy loss between the generated ROSs and luminol, but availably immobilize luminol on the sensing interface *via* covalent bond and electrostatic interaction.

MicroRNAs (miRNAs), which acted as ideal biomarkers in cancer initiation and progression, are significant for cancer surveillance (Causa et al., 2015; J.B. Li et al., 2016). This study fabricated an ultrasensitive ECL biosensor for miRNA-21 detection through L-Au NPs@ZnO nanomaterials as an ECL probe and dissolved O_2 as endogenous coreactant. Firstly, chitosan was employed to immobilize the L-Au NPs@ZnO nanomaterials into sensing interface due to its biocompatibility and film-forming properties (Zhang et al., 2017), and then Ag NPs were modified for anchoring thiol-modified hairpin DNA (H1) *via* Ag-S bond (You et al., 2018; Zhang et al., 2018). Then target miRNA-21 was introduced to open the hairpins H1. Afterwards, with the addition of H2 and H3, the hybridization chain reaction (HCR) was realized through hairpin polymerization to generate DNA dendrimers modified substantial Fc. Subsequently, when Fc consumed coreactant dissolved O_2 (Cao et al., 2006; Li et al., 2014; Liu et al., 2018; Zhou et al., 2017), the ECL signal was restricted to result in a lower ECL intensity. As a result, a luminol-based bioanalysis strategy manifested high sensitivity of miRNA-21 detection. Thus, this work proposed an effective method for signal amplification of ECL biosensors, which afforded an ultrasensitive platform for the detection of biomolecules and clinical diagnosis.

2. Experiment section

2.1. Preparation of L-Au NPs@ZnO

Initially, luminol-functionalized Au NPs (L-Au NPs) were synthesized by a general method (Zhang et al., 2014). First of all, 5 mL $HAuCl_4{\cdot}4H_2O$ (0.25 mM) and 1 mL luminol (12.5 mM) was added into beaker to obtain L-Au NPs complexes in ice bath (the detailed optimized experimental of luminol concentration was shown in the Supporting Information). Then 0.15 mL $NaBH_4$ (0.1 M) was injected dropwise to reduce $HAuCl_4{\cdot}4H_2O$ to Au NPs. Luminol with a positive group -NH_2 was bonded to Au NPs via electrostatic interaction and Au-N bond (Wang et al., 2015). The L-Au NPs solution with negative charge was acquired after ice bath for 10 min and continuous stirring for 6 h under ambient temperature. The resultant solution was preserved at 4 °C.

Simultaneously, the synthesis process of ZnO nanostars was shown in the Supporting Information. Briefly, positively charged ZnO nanostars were constructed by dispersing 1 mL ZnO nanostars into 4 mL 0.20% poly-(diallyldimethylammonium chloride) (PDDA) aqueous solution containing Tris (20 mM) and NaCl (20 mM) (Du et al., 2011). Afterwards, the solution was dispersed by ultrasonic and kept agitating for 2 h under ambient temperature, and then it was centrifugated and cleaned with deionized water for several times. Subsequently, the obtained ZnO sediments were dispersed in L-Au NPs solution by ultrasonic and then kept stirring for 4 h to obtain the L-Au NPs@ZnO due to the electrostatic interaction. Finally, the L-Au NPs@ZnO solution was centrifuged and washed several times with water. The synthesis process of L-Au NPs@ZnO was displayed in Scheme 1A.

2.2. Fabrication of biosensor

The GCE (Φ = 4 mm) was respectively polished with 0.3 and 0.05 μm alumina powder and cleaned by deionized water for further use. Firstly, 5 μL L-Au NPs@ZnO, 10 μL 0.5% chitosan, and 10 μL Ag NPs (the preparation process of Ag NPs was exhibited in Supporting Information) were modified on electrode surface successively. Then 10 μL H1 (2 μM) was incubated on the modified sensing interface for 12 h at 4 °C through Ag-S bond. After rinsing, 10 μL hexanethiol (HT, 1 mM) was introduced to resist the nonspecific adsorption for 40 min at room temperature. Afterwards, 10 μL miRNA-21 of different concentration were dripped for incubating 2 h to hybridize with H1. Ultimately, 10 μL H2 (2 μM) and 10 μL H3 (2 μM) modified a large number of Fc were dripped and incubated for 2 h. The fabrication process of developed biosensor was displayed at Scheme 1B. The characterization of the biosensor assembly process was investigated by electrochemical impedance spectroscopy (EIS) and related EIS graph was shown in Fig. S1.

2.3. ECL detection

The proposed biosensor was measured in 2 mL air-saturated phosphate buffer saline (PBS, 0.1 M, pH = 7.4). A high voltage of 800 V was provided to the photomultiplier tube (PMT) with the magnitude as 3, and the working potential was carried out from −0.6 – 0.8 V with scanning speed of 500 mV/s. The $\triangle I$ was the decreased value ($\triangle I = I_0 - I$, I_0 represented the ECL signal of blank, while I represented the ECL signal with different concentration of miRNA-21).

3. Results and discussion

3.1. Characterization of ZnO and L-Au NPs@ZnO

The scanning electron microscope (SEM) pattern of ZnO was displayed in Fig. 1A, it showed that ZnO has the morphology like stars with a length of about 300 nm. The X-ray diffraction (XRD) was utilized for further confirming the synthesis of ZnO, as exhibited in Fig. 1C, the peak values at 31.8, 34.4, 36.3, 47.54, 56.6, 62.86, 67.98 (a) could correspond to (100), (002), (101), (102), (110), (103), and (112) standard PDF card of ZnO crystal planes (b), demonstrating ZnO was hexagonal phase (Han et al., 2015).

Meantime, the morphology of the as-synthesized L-Au NPs@ZnO was characterized by transmission electron microscope (TEM). From Fig. 1B, the ZnO has the star-like morphology with a diameter of 300 nm, and the small particles decorated on surface portion of the rods were L-Au NPs of about 5 nm in size. The elemental analysis of L-Au NPs@ZnO was investigated by X-ray photoelectron spectroscopy (XPS). According to Fig. 1D, the peaks at about 1020.61 eV, 530.34 eV, 499.38 eV, 399.53 eV, 284.8 eV, 88 eV could respectively ascribe to Zn 2p, O 1s, Zn LM2, N 1s, C 1s, and Au 4f, verifying the L-Au NPs@ZnO nanomaterials were triumphantly synthesized.

3.2. The possible mechanism of the ECL emitting process

Relative experiments were performed to demonstrate the ECL emission process of luminol-O_2 system. From Fig. 2A, when 5 μL L-Au NPs@ZnO were dripped on the electrode, a distinguished ECL intensity peak about 7081 a.u. (curve a) was observed in air-saturated PBS, while Au NPs@ZnO/GCE had no distinct ECL peak (Fig. S4B), stating that the ECL emission was actually generated only in the presence of luminol. Simultaneously, the matching cyclic voltammogram (CV) curve (Fig. 2B, curve a) showed reduction and oxidation peak which respectively assigned to −0.06 V and 0.2 V owing to the reaction of dissolved O_2 on ZnO surface (X. Li et al., 2016; Katerina et al., 2019; Yoshio and Atsuko, 2017). After ventilating with highly pure Ar for 10 min to remove the dissolved O_2 around ZnO in the PBS, the ECL emission conspicuously decreased (Fig. 2A, curve b). However, L-Au NPs@ZnO/GCE was immersed in the Ar-saturated PBS including 320 μM H_2O_2, which was equivalent to the concentration of dissolved O_2 at 25 °C (Zhou

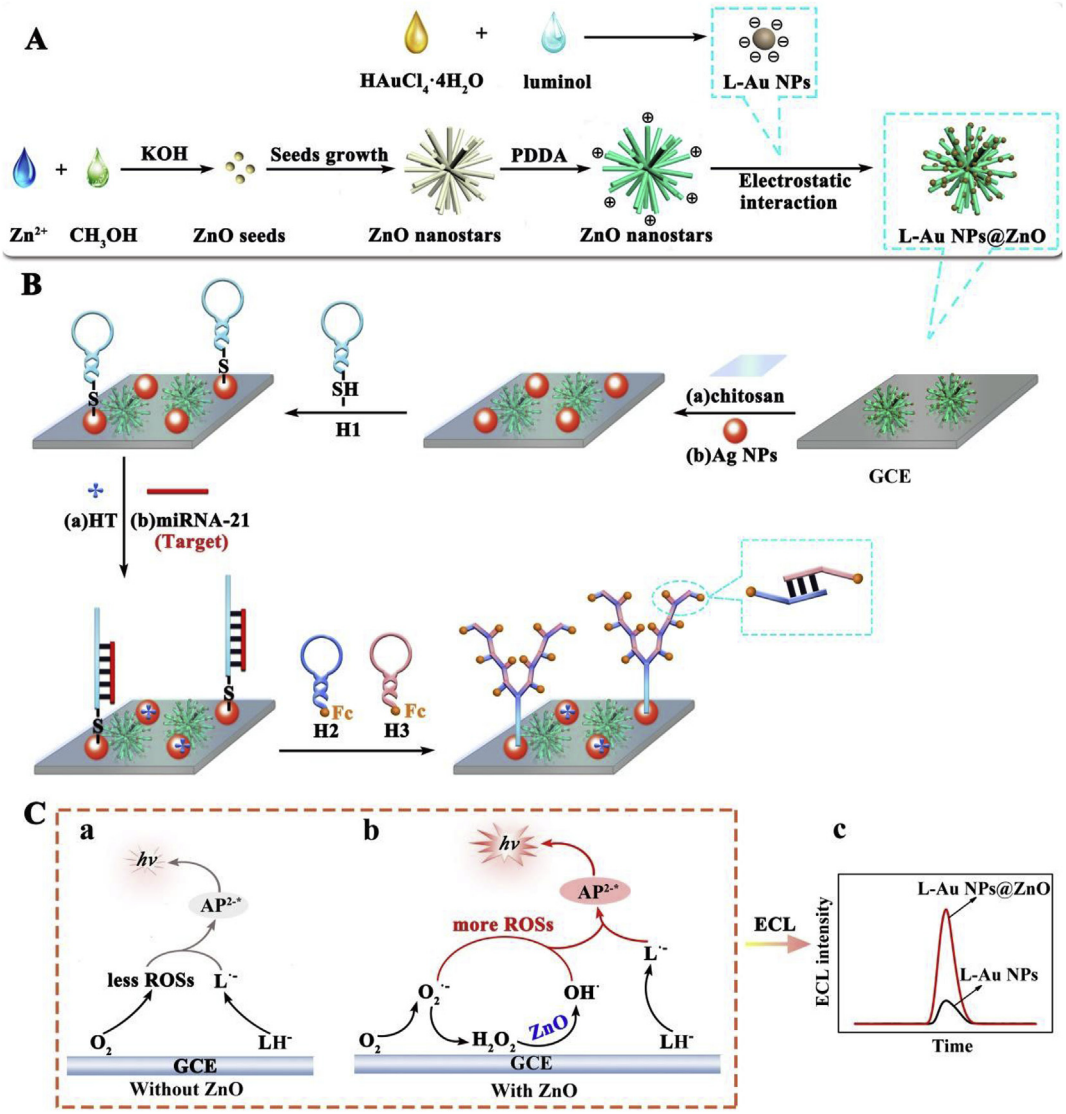

Scheme 1. (A) The synthesis process of L-Au NPs@ZnO materials. (B) The fabrication process of the developed biosensor for miRNA-21 detection. (C) Possible mechanism of luminol-O_2 system without (a) and with coreaction accelerator ZnO (b), ECL response of L-Au NPs, L-Au NPs@ZnO (c).

et al., 2017), the ECL signal was 4330 a.u. (Fig. 2A, curve c). Thus the dissolved O_2 exactly served as coreactant during the emission of luminol. Moreover, superoxide dismutase (SOD) which acted as an efficient and specific scavenges of superoxide ($O_2^{\bullet -}$) radicals was added into the air-saturated PBS (Fig. 2A, curve d) (He et al., 2016; Learman et al., 2011), an ECL intensity at 3409 a.u. was observed. And with the correspondent CV response, an oxidation peak at 0.18 V (Fig. 2B, curve b) was obtained, which implied the existence of hydroxyl ($OH^{\bullet}$) species during the ECL emission. Successively, L-cysteine (1 mM) as annihilation reagent of $OH^{\bullet}$ and $O_2^{\bullet -}$ radicals was added into air-saturated PBS to distinctly quench the ECL signal (Fig. 2A, curve e) (Deng et al., 2011; Wang et al., 2016). Meantime, the CV showed no distinct peaks at −0.06 V and 0.2 V around (Fig. 2B, curve c).

In conclusion, for luminol-O_2 system with ZnO, luminol anionic radicals ($L^{\bullet -}$) could be generated through the oxidation of luminol anions (LH^-). Then on the cathode, superoxide anion ($O_2^{\bullet -}$) could be obtained through the reduction of dissolved O_2 on ZnO surface, and the $O_2^{\bullet -}$ could produce hydrogen peroxide (H_2O_2), which could produce full or partly $OH^{\bullet}$ on the anode. Afterwards, the generated $L^{\bullet -}$ in situ reacted with the generated $O_2^{\bullet -}$ and $OH^{\bullet}$, leading to more excited state species of luminol (AP^{2-*}) for enhancing ECL intensity dramatically (Scheme 1C, b).

3.3. Analytical performance of the ECL biosensor toward miRNA-21

The sensitivity of the biosensor was determined by different concentrations of target miRNA-21. As demonstrated in Fig. 3A, the ECL intensity decreased along with the increase of miRNA-21 concentration from 100 aM to 100 pM. The results in Fig. 3B showed that the $\triangle I$ which was the decreased value increased linearly with the logarithm of miRNA-21 concentration in scope of 100 aM - 100 pM. The regression equation was $\triangle I = 770.89 \lg c + 13437$ with a correlation coefficient of 0.99447. Additionally, the LOD was calculated to be 18.6 aM (the detailed calculation process of LOD was presented in the Supporting Information). As displayed in Table 1, the elaborated biosensor showed a relative wider linear rang with a lower LOD, which indicated it might have great promising for ultimate application in clinical bioassay.

To estimate the selectivity of the biosensor for miRNA-21 detection, miRNA-122, miRNA-141 and miRNA-155 were selected as the interfering substances. The concentration of interfering substances (1 nM) was 100 times higher than target miRNA-21 (10 pM). As depicted in Fig. 3C, the ECL signal of interferences not only exhibited slight changes compared with the blank samples, but displayed a distinct difference with 10 pM miRNA-21. Meantime, the ECL intensity of 10 pM miRNA-21 was close to mixture, while it showed great change compared to

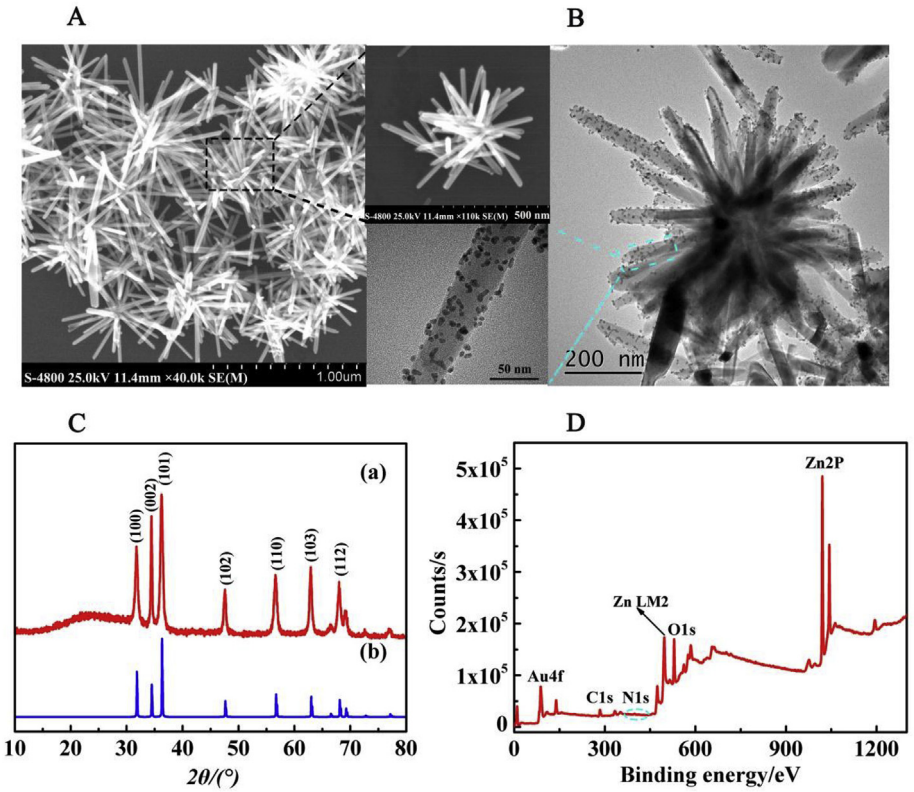

Fig. 1. (A) The SEM image of ZnO. (B) The TEM image of L-Au NPs@ZnO, and the insets of A and B showed the magnified SEM image of ZnO and the amplified TEM image of L-Au NPs@ZnO, respectively. (C) XRD patterns of (a) the ZnO and (b) the standard PDF card of ZnO crystal. (D) The XPS spectra of L-Au NPs@ZnO.

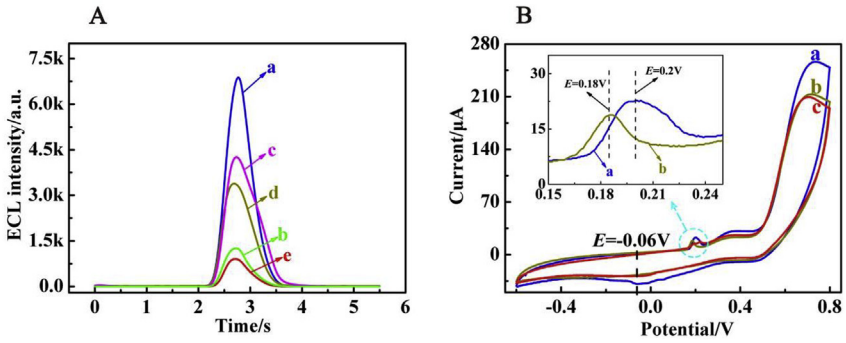

Fig. 2. (A) ECL characterization of L-Au NPs@ZnO modified GCE in (a) air-saturated, (b) Ar-saturated, (c) Ar-saturated PBS with the addition of 320 μM H_2O_2, (d) air-saturated PBS with the addition of SOD, (e) air-saturated PBS with the addition of 1 mM L-cysteine. (B) The CV curves of L-Au NPs@ZnO modified GCE in (a) air-saturated PBS, (b) air-saturated PBS with the addition of SOD, (c) air-saturated PBS with the addition of 1 mM L-cysteine, and the illustration showed the amplified CV curves of (a) and (b).

blank samples. All above results implied the proposed biosensor was provided with superior selectivity of miRNA-21.

As illustrated in Fig. 3D, under successional scanning for 10 cycles at 10 pM miRNA-21 in PBS, the ECL signal showed inconspicuous fluctuation and the relative standard deviation (RSD) was calculated as 2.46%, which manifested the excellent stability of the proposed biosensor.

3.4. The pragmatic application of biosensor

To evaluate the feasibility of proposed biosensor to real samples in development of miRNA analysis, human breast cancer cell (MCF-7) with high-expressed miRNA-21, and human cervical cancer cell (Hela) with low-expressed miRNA-21 were chosen to measure the expression of miRNA-21. According to Fig. 4, the ECL intensity of 10^3 Hela cells were close to blank and 10^3 MCF-7 cells were lower than blank. The ECL response signal of MCF-7 increased with the gradually decreasing cell numbers, while the signal of Hela increased more obvious with the decrease of cell numbers. The results suggested that the developed biosensor could monitor miRNA from tumor cells.

4. Conclusion

In summary, the luminol-centric ECL biosensor was first developed for ultrasensitively detecting miRNA-21 based on ZnO as coreaction accelerator and dissolved O_2 as coreactant. Firstly, luminol was directly modified on the surface of ZnO, which shortened electronic transmission distance and reduced energy loss, resulting in higher coreaction acceleration efficiency of ZnO to luminol-O_2 system. Secondly, ZnO was employed as a new coreaction accelerator to accelerate the reduction of the dissolved O_2 for significantly enhancing the ECL efficiency of luminol, realizing the ultrasensitive detection of miRNA-21 in cancer cells with a low detection limit down to attomolar level. Overall, this work proposed a new coreaction accelerator strategy to luminol-O_2 system for cancer biomarker monitoring, which hold great potential for ultimate applications in clinical diagnosis.

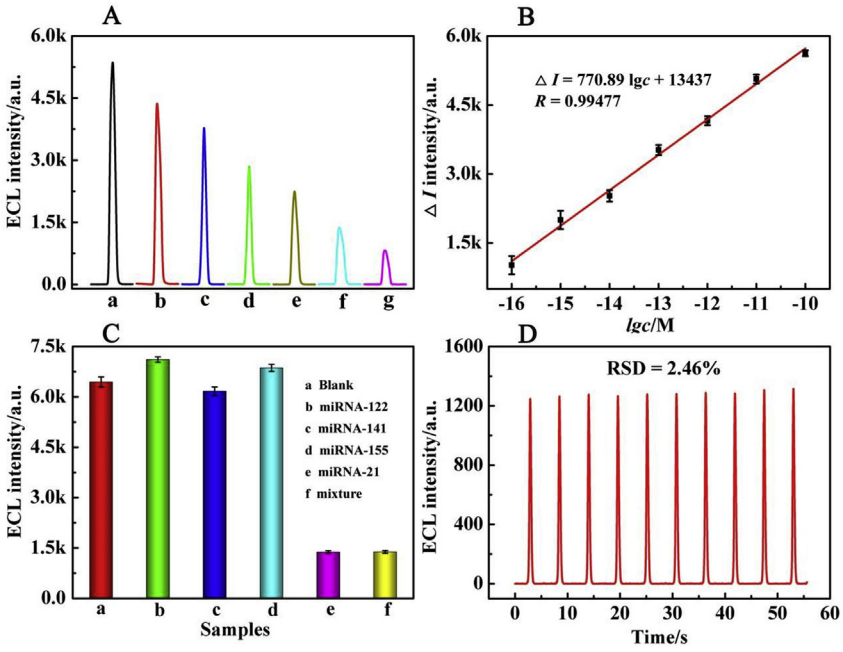

Fig. 3. (A) ECL responses of the biosensor with various miRNA-21 concentration: 100 aM, 1 fM, 10 fM, 100 fM, 1 pM, 10 pM, 100 pM (from curve a to g). (B) The calibration curve of miRNA-21 detection. (C) Selectivity of the biosensor for miRNA-21 (10 pM) detection against the interference miRNAs: (a) Blank, (b) miRNA-122 (1 nM), (c) miRNA-141 (1 nM), (d) miRNA-155 (1 nM), (e) miRNA-21 (10 pM), (f) mixture (containing 1 nM miRNA-122, 1 nM miRNA-141, 1 nM miRNA-155, 10 pM miRNA-21). (D) Stability of the developed biosensor with the presence of miRNA-21 (10 pM).

Table 1
Comparison of this approach with other strategies.

Method	Target	Linear range	LOD	Ref.
Fluorescence	miRNA-21	1 fM ~ 50 pM	0.27 fM	Yin et al. (2017)
Fluorescence	miRNA-155	100 fM ~ 1 pM	33.4 fM	Miao et al. (2018)
Electrochemistry	miRNA-21	10 fM ~ 1 pM	4.53 fM	Shi et al. (2018)
SERS	miRNA-133a	1 fM ~ 10 nM	0.306 fM	Sun and Li (2018)
ECL	miRNA-319a	0.5 fM ~ 1 pM	0.14 fM	Wang et al. (2018)
ECL	miRNA-141	1 fM ~ 10 pM	0.4 fM	Lu et al. (2018)
ECL	miRNA-21	100 aM ~ 100 pM	18.6 aM	this work

SERS: Surface-Enhanced Raman Scattering.

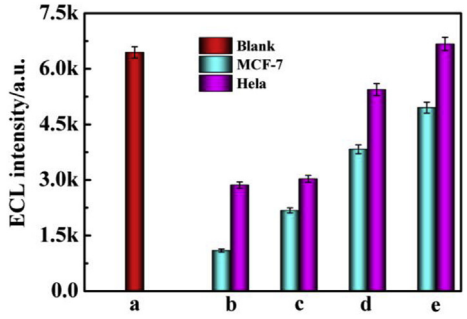

Fig. 4. Analysis of the miRNA-21 in different tumor cells detection (a) blank; (b) 10^6 cells; (c) 10^5 cells; (d) 10^4 cells; (e) 10^3 cells of MCF-7 and Hela.

Declaration of interests

The authors declare that they have no known competing financial interests or personal relationships that could have appeared to influence the work reported in this paper.

CRediT authorship contribution statement

Xiaoli Zhang: Conceptualization, Data curation, Formal analysis, Investigation, Writing - original draft, Writing - review & editing. **Weimin Li:** Data curation, Investigation. **Ying Zhou:** Conceptualization, Writing - original draft, Supervision. **Yaqin Chai:** Funding acquisition, Resources, Project administration, Supervision. **Ruo Yuan:** Funding acquisition, Resources, Writing - review & editing.

Acknowledgements

This work was financially supported by the NNSF of China (21775124, 21575116, 21675129), and the Fundamental Research Funds for the Central Universities (XDJK2018AA0003), China.

Appendix A. Supplementary data

Chemicals and materials, apparatus, preparation of ZnO nanostars, preparation of Ag NPs, the characterization of the electrode assembly process, experimental condition optimization, the UV–vis absorption spectra of L-Au NPs, the signal comparison of different ECL probes, PAGE analysis, the UV–vis and fluorescence spectra of L-Au NPs@ZnO, limit of detection calculation.

Supplementary data to this article can be found online at https://doi.org/10.1016/j.bios.2019.04.004.

References

Cao, W.D., Ferrance, J.P., Demas, J., Landers, J.P., 2006. J. Am. Chem. Soc. 128, 7572–7578.
Causa, F., Aliberti, A., Cusano, A.M., Battista, E., Netti, P.A., 2015. J. Am. Chem. Soc. 137, 1758–1761.
Cui, H., Wang, W., Duan, C.F., Dong, Y.P., Guo, J.Z., 2007. Chem. Eur J. 13, 6975–6984.
Deng, S.Y., Hou, Z.T., Lei, J.P., Lin, D.J., Hu, Z., Yan, F., Ju, H.X., 2011. Chem. Commun. 47, 12107–12109.
Du, D., Tao, Y., Zhang, W.Y., Liu, D.L., Li, H.B., 2011. Biosens. Bioelectron. 26, 4231–4235.
Gu, W.L., Deng, X., Gu, X.X., Jia, X.F., Lou, B.H., Zhang, X.W., Li, J., Wang, E.K., 2015. Anal. Chem. 87, 1876–1881.
Han, C., Chen, Z., Zhang, N., Colmenares, J.C., Xu, Y.J., 2015. Adv. Funct. Mater. 25, 221–229.
Hao, N., Zhang, X., Zhou, Z., Hua, R., Zhang, Y., Liu, Q., Qian, J., Li, H.N., Wang, K., 2017. Biosens. Bioelectron. 97, 377–383.
He, W., Kim, H.K., Wamer, W.G., Melka, D., Callahan, J.H., Yin, J.J., 2014. J. Am. Chem. Soc. 136, 750–757.
He, W.W., Jia, H.M., Cai, J.H., Han, X.N., Zheng, Z., Wamer, W.G., Yin, J.J., 2016. J. Phys. Chem. C 120, 3187–3195.
Katerina, G., Andreas, S., Spyros, N.Y., Stylianos, G.N., 2019. Electrochim. Acta 298, 587–598.
Learman, D.R., Voelker, B.M., Vazquez-Rodriguez, A.I., Hansel, C.M., 2011. Nat. Geosci. 4, 95–98.
Lei, Y.M., Wen, R.X., Zhou, J., Chai, Y.Q., Yuan, R., Zhuo, Y., 2018. Anal. Chem. 90, 6851–6858.
Li, F., Yu, Y.Q., Li, Q., Zhou, M., Cui, H., 2014. Anal. Chem. 86, 1608–1613.
Li, J.B., Huang, L., Xiao, X., Chen, Y.J., Wang, X.X., Zhou, Z.Q., Zhang, C.Y., Zhang, Y., 2016. J. Am. Chem. Soc. 138, 15943–15949.
Liu, J., Ren, J., Bao, X.J., Gao, W., Wu, C.L., Zhao, Y.B., 2016. Anal. Chem. 88, 5865–5870.
Liu, J.L., Tang, Z.L., Zhang, J.Q., Chai, Y.Q., Zhuo, Y., Yuan, R., 2018. Anal. Chem. 90, 5298–5305.
Lu, H.J., Pan, J.B., Wang, Y.Z., Ji, S.Y., Zhao, W., Luo, X.L., Xu, J.J., Chen, H.Y., 2018. Anal. Chem. 90, 10434–10441.
Li, X., Yu, J.G., Jaroniec, M., 2016. Chem. Soc. Rev. 45, 2603–2636.
Miao, X.M., Cheng, Z.Y., Ma, H.Y., Li, Z.B., Xue, N., Wang, P., 2018. Anal. Chem. 90, 1098–1103.
Qiao, Y., Li, Y., Fu, W., Guo, Z., Zheng, X., 2018. Anal. Chem. 90, 9629–9636.
Richter, M.M., 2004. Chem. Rev. 104, 3003–3036.
Shi, L., Mu, C.L., Gao, T., Chen, T.S., Hei, S., Yang, J., Li, G.X., 2018. Chem. Commun. 54, 11391–11394.
Sirelkhatim, A., Mahmud, S., Seeni, A., Kaus, N.H.M., Ann, L.C., Bakhori, S.K.M., Hasan, H., Mohamad, D., 2015. Nano-Micro Lett. 7, 219–242.
Sun, Y.D., Li, T., 2018. Anal. Chem. 90, 11614–11621.
Sun, Y.Y., Wu, X.H., Zhang, K., Ren, Q.X., Xie, R.G., 2018. Biosens. Bioelectron. 100, 445–452.
Wang, J.X., Zhuo, Y., Zhou, Y., Yuan, R., Chai, Y.Q., 2015. Biosens. Bioelectron. 71, 407–413.
Wang, L., Tricard, S., Yue, P.W., Zhao, J.H., Fang, J., Shen, W., 2016. Biosens. Bioelectron. 77, 1112–1118.
Wang, M.H., Zhou, Y.L., Yin, H.S., Jiang, W.J., Wang, H.Y., Ai, S.Y., 2018. Biosens. Bioelectron. 107, 34–39.
Wu, F.F., Zhou, Y., Zhang, H., Yuan, R., Chai, Y.Q., 2018. Anal. Chem. 90, 2263–2270.
Yin, H.S., Li, B.C., Zhou, Y.L., Wang, H.Y., Wang, M.H., Ai, S.Y., 2017. Biosens. Bioelectron. 96, 106–112.
Yoshio, N., Atsuko, Y.N., 2017. Chem. Rev. 117, 11302–11336.
You, M., Yang, S., Tang, W.X., Zhang, F., He, P.G., 2018. Biosens. Bioelectron. 112, 72–78.
Zhang, H.R., Wu, M.S., Xu, J.J., Chen, H.Y., 2014. Anal. Chem. 86, 3834–3840.
Zhang, L., Yang, W., Tao, K., Tao, K.X., Song, Y., Xie, H.J., Wang, J., Li, X.L., Shuai, X.M., Gao, J.B., Chang, P.P., 2017. ACS Appl. Mater. Interfaces 9, 3432–3444.
Zhang, X.H., Qian, Y.X., Ma, X.J., Xia, M.F., Li, S.Q., Zhang, Y.D., 2018. Nanoscale 10, 76–81.
Zhou, Y., Wang, H.J., Zhuo, Y., Chai, Y.Q., Yuan, R., 2017. Anal. Chem. 89, 3732–3738.